Asymmetric backscattering from the hybrid magneto-electric meta particle

Cite as: Appl. Phys. Lett. **109**, 203503 (2016); https://doi.org/10.1063/1.4967238
Submitted: 21 August 2016 . Accepted: 25 October 2016 . Published Online: 18 November 2016

Vitali Kozlov, Dmitry Filonov, Alexander S. Shalin, Ben Z. Steinberg, and Pavel Ginzburg

Asymmetric backscattering from the hybrid magneto-electric meta particle

Vitali Kozlov,[1,a),b)] Dmitry Filonov,[1,2,b)] Alexander S. Shalin,[2] Ben Z. Steinberg,[1] and Pavel Ginzburg[1,2]
[1]*School of Electrical Engineering, Tel Aviv University, Tel Aviv 69978, Israel*
[2]*ITMO University, St. Petersburg 197101, Russia*

(Received 21 August 2016; accepted 25 October 2016; published online 15 November 2016)

The optical theorem relates the total scattering cross-section of a given structure with its forward scattering, but does not impose any restrictions on other directions. Strong backward-forward asymmetry in scattering could be achieved by exploring retarded coupling between particles, exhibiting both electric and magnetic resonances. Here, a hybrid magneto-electric particle (HMEP), consisting of a split ring resonator acting as a magnetic dipole and a wire antenna acting as an electric dipole, is shown to possess asymmetric scattering properties. When illuminated from opposite directions with the same polarization of the electric field, the structure has exactly the same forward scattering, whereas the backward scattering is drastically different. The scattering cross section is shown to be as low as zero at a narrow frequency range when illuminated from one side, while being maximal at the same frequency range when illuminated from the other side. Theoretical predictions of the phenomena are supported with both numerical and experimental conformations, obtained at the GHz frequency range, and all are in a good agreement with each other. HMEP meta-particles could be used as building blocks for various metamaterials assembling solar cells, invisibility cloaks, holographic masks, etc. *Published by AIP Publishing.*
[http://dx.doi.org/10.1063/1.4967238]

Metamaterials have gained broad interest in the past decade, as they hold the promise for delivering new types of devices.[1] Some of the more notable applications are solar cells,[2] invisibility cloaking devices,[3] holography,[4] opto-mechanics,[5,6] etc. The basic functionalities of metamaterials are achieved by carefully designing the constitutive elements (meta-atoms) that govern the composite's behavior. Split ring resonators (SRR) and thin wires are often employed as the building blocks in many realizations, owing both to the fact that these structures are well understood theoretically,[7] as well as the relative ease of their manufacturing. In order to achieve complex properties, meta-atoms often consist of more than one structure.[8–11] One of the desirable functionalities that could be achieved with metamaterials is an asymmetric response. For example, asymmetric properties (and especially transmission) could find use in a range of applications, such as antireflection coatings,[12] light harvesting in solar cells,[13] directional color routing,[14] polarization sensitive devises,[15,16] and photonic diodes[17] to name a few.

Scattering characteristics of individual elements could be controlled by engineering their multipolar responses. For example, the so-called Huygen's elements rely on the interference between electric and magnetic dipolar responses that suppress the backward scattering.[18,19] The properties of magnetic and electric resonances could be tailored by particle's shape, e.g., core-shell geometry.[20] Meta-particles with nonsymmetrical scattering are discussed in details in Refs. 21–24, where a few structures were studied analytically, including the omega, omega-Tellegen, and the chiral-moving particle. It was shown that periodic structures constructed from such meta-atoms could be used to create thin films with tunable nonsymmetrical transmission and reflection, e.g., Ref. 25 and references therein. Here, another example of asymmetric meta-particle is proposed, emphasising on reflection characteristics and its balance with the forward scattering.

The optical theorem[26] relates the forward scattering from an object with its total radar cross-section (RCS) and is a manifestation of the fundamental principle of causality. Remarkably, the theorem favors the forward direction over all the rest, and there is no simple relation between the total RCS and the backward scattering, for example. Here, a special type of meta-atom, having a symmetric forward and asymmetric backward scattering, is studied. The hybrid magneto-electric particle (HMEP), consisting of a SRR and a thin wire (Fig. 1), is considered analytically, numerically, and experimentally. The HMEP is shown to have asymmetric backscattering when illuminated by a plane wave from opposite directions. It is worth noting that related structures have been previously analyzed in Refs. 27 and 28, whereas theoretical descriptions were reported in Ref. 9, where the HMEP was used to construct narrow band filters. Intuitively, the asymmetric reflection of the HMEP could be understood by observing Fig. 1. It essentially stems from the coupling mechanism between the two HMEP constituents, namely, between the electric dipole (ED) and the magnetic dipole (MD). The ED couples to the MD via its own magnetic field whose spatial distribution along the z-axis is an odd function of z. Likewise, the MD couples to the ED via its own electric field whose spatial distribution along z is again an odd function of z. Hence, the ED-MD couplings change sign when d flips sign, as can be seen by comparing the ED magnetic field

[a)]vitaliko@mail.tau.ac.il
[b)]V. Kozlov and D. Filonov contributed equally to this work

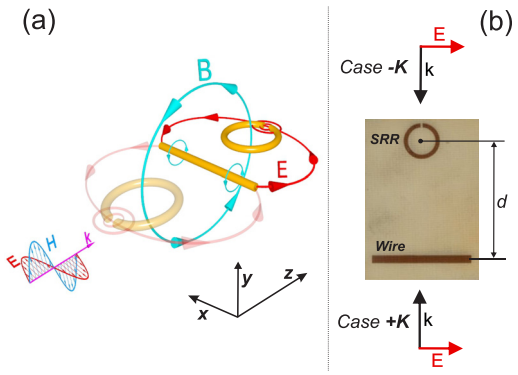

FIG. 1. Hybrid magneto-electric particle (HMEP) geometry. (a) Perspective view of the structure and the coupling fields. Electric field of the ring represented with the red line, whereas magnetic field of the wire is of turquoise color. The semi-transparent ring corresponds to changing particle's orientation in respect to the incident field. (b) Top view of the fabricated structure (photographic image). Forward $(+k)$ and backward $(-k)$ propagation directions are equivalent to changing the sign of d, while keeping the incident wave constant.

at the SRR and at the semi-transparent SRR in Fig. 1(a). Two factors contribute to the excitation of each of the HMEP constituents. One is the incident field. The second is the aforementioned coupling mechanism. The degree of asymmetry is mainly determined by the relative strengths of these two factors and it depends on frequency, inter-particle distance, and the individual parameters of the ED and MD.

The letter is organized as follows—first a theoretic framework is derived to show that asymmetric behavior is to be expected for the coupled dipoles. Next, numeric modeling is performed, and an optimized structure is compared with experimental results in the GHz range.

Electromagnetic scattering from a structure could be approached with the help of the multipolar decomposition technique.[26] Subwavelength scatterers could often be approximated analytically with a few of the leading (dipolar) terms and the related polarizabilities, which could be calculated directly from the geometry and material composition of the structure. When a structure (meta-atom hereafter) consists of several subwavelength features, the scattering problem could be solved self-consistently by employing the coupled dipoles technique.[29,30]

In the general case, both electric ($\boldsymbol{p}$) and magnetic ($\boldsymbol{m}$) moments could be attributed to each subwavelength scatterer, illuminated by an incident electric $\boldsymbol{E^{inc}}$ and magnetic $\boldsymbol{H^{inc}}$ fields. Matrix equation for a set of discrete coupled dipoles, labeled with sub index "i" and situated at points $\boldsymbol{r_i}$, is given in Eq. (1),

$$\begin{bmatrix} \boldsymbol{p_i} \\ \boldsymbol{m_i} \end{bmatrix} = \begin{bmatrix} \boldsymbol{a}^i_{ee} & \boldsymbol{a}^i_{em} \\ \boldsymbol{a}^i_{me} & \boldsymbol{a}^i_{mm} \end{bmatrix} \left(\sum_{\substack{j=1 \\ j\neq i}}^{N} \begin{bmatrix} \epsilon_0{}^{-1}\boldsymbol{A}(\boldsymbol{r_i},\boldsymbol{r_j}') & -\mu_0\boldsymbol{B}(\boldsymbol{r_i},\boldsymbol{r_j}') \\ \boldsymbol{B}(\boldsymbol{r_i},\boldsymbol{r_j}') & \boldsymbol{A}(\boldsymbol{r_i},\boldsymbol{r_j}') \end{bmatrix} \times \begin{bmatrix} \boldsymbol{p_j} \\ \boldsymbol{m_j} \end{bmatrix} + \begin{bmatrix} \boldsymbol{E^{inc}}(\boldsymbol{r_i}) \\ \boldsymbol{H^{inc}}(\boldsymbol{r_i}) \end{bmatrix} \right), \tag{1}$$

where ε_0 and μ_0 are the free space permittivity and permeability, $\boldsymbol{a}^i_{XX'}$ is a 3×3 matrix for the electric, magnetic, or magneto-electric polarizability of scatterer i, whereas $\boldsymbol{A}(\boldsymbol{r},\boldsymbol{r}')$ and $\mathrm{B}(\boldsymbol{r},\boldsymbol{r}')$ are the dyadic Green's functions given by the following equation:

$$\begin{aligned} \boldsymbol{A}(\boldsymbol{r},\boldsymbol{r}') &= G(R)\left[k^2(\boldsymbol{I}-\boldsymbol{N}) + \left(\frac{1}{R^2}+\frac{jk}{R}\right)(3\boldsymbol{N}-\boldsymbol{I})\right], \\ \boldsymbol{B}(\boldsymbol{r},\boldsymbol{r}') &= ck^2G(R)\left[1+\frac{1}{jkR}\right]\boldsymbol{N}^{(v)}, \end{aligned} \tag{2}$$

where $\mathbf{I}$ is the 3×3 identity matrix, $R=|\boldsymbol{r}-\boldsymbol{r}'|$, $G(R)=\frac{e^{-jkR}}{4\pi R}$, $\boldsymbol{N}=[\hat{\boldsymbol{n}}^T\hat{\boldsymbol{n}}]$, $\boldsymbol{N}^{(v)}=[(\hat{\boldsymbol{n}}\times\hat{\boldsymbol{x}})^T,(\hat{\boldsymbol{n}}\times\hat{\boldsymbol{y}})^T,(\hat{\boldsymbol{n}}\times\hat{\boldsymbol{z}})^T]$, $\hat{\boldsymbol{n}}=\frac{\boldsymbol{r}-\boldsymbol{r}'}{|\boldsymbol{r}-\boldsymbol{r}'|}$, and k is the free space wave vector. Eq. (1) has a $6N\times6N$ matrix form (N is the total number of particle scatterers), which could be solved by inversion to find the dipole moments of each scatterer.

In the special case of two simple scatterers and the coordinate system depicted in Fig. 1, the SRR's polarizability may be approximated as being dependent only on $\boldsymbol{a}^{SRR}_{mm}$, whereas the wire's polarizability only on $\boldsymbol{a}^{Wire}_{ee}$,

$$\boldsymbol{a}^{SRR}_{mm} = \begin{pmatrix} 0 & 0 & 0 \\ 0 & a_{SRR} & 0 \\ 0 & 0 & 0 \end{pmatrix}, \quad \boldsymbol{a}^{Wire}_{ee} = \begin{pmatrix} a_{Wire} & 0 & 0 \\ 0 & 0 & 0 \\ 0 & 0 & 0 \end{pmatrix}. \tag{3}$$

The resulting dipolar moments, excited with a plane wave illumination, are

$$\begin{aligned} \boldsymbol{p}^{Wire} &= a_{Wire}\frac{1-Sign(d)\mu_0 a_{SRR}\eta^{-1}ve^{-jkd}}{1+\mu_0 a_{Wire}a_{SRR}v^2}\hat{\boldsymbol{x}}, \\ \boldsymbol{m}^{SRR} &= a_{SRR}\frac{Sign(d)a_{Wire}v+\eta^{-1}e^{-jkd}}{1+\mu_0 a_{Wire}a_{SRR}v^2}\hat{\boldsymbol{y}}, \end{aligned} \tag{4}$$

where η is the free space impedance and v is the retarded coupling constant related to Green's dyadic given by $v=ck^2\frac{e^{-jk|d|}}{4\pi|d|}(1+\frac{1}{jk|d|})$. The derivation utilizes the HMEP geometry, where the wire is located at the origin and the ring is displaced by the distance d along the z-axis (i.e., at z = d), which could be either positive or negative. Changing the sign of d is analogous to changing the propagation direction of the incident wave. The term $Sign(d)$ explicitly appears in Eq. (4), underlining the dependence of the dipole moments on the HEMP orientation (or propagation direction). The appearance of the phase delay e^{-jkd} and $Sign(d)$ term has the origin in magneto-electric coupling. This is the core property for the asymmetry effect that cannot be achieved in a similar fashion with two purely electrical coupled dipoles in subwavelength geometry.

The scattered field is extracted from the dipolar moments and is given by the following equation:

$$\begin{bmatrix} \boldsymbol{E^{sc}}(\boldsymbol{r}) \\ \boldsymbol{H^{sc}}(\boldsymbol{r}) \end{bmatrix} = \sum_{j=SRR,Wire} \begin{bmatrix} \epsilon_0{}^{-1}\boldsymbol{A}(\boldsymbol{r},\boldsymbol{r_j}') & -\mu_0\boldsymbol{B}(\boldsymbol{r},\boldsymbol{r_j}') \\ \boldsymbol{B}(\boldsymbol{r},\boldsymbol{r_j}') & \boldsymbol{A}(\boldsymbol{r},\boldsymbol{r_j}') \end{bmatrix} \begin{bmatrix} \boldsymbol{p_j} \\ \boldsymbol{m_j} \end{bmatrix}. \tag{5}$$

Direct calculation of the forward and backward scattering could be performed by substituting the relevant numbers in Eq. (5). For example, referring to Fig. 1, the backward and the forward-scattered far-fields along the z-axis ($k|z|\to\infty$) are given, respectively, by

$$\boldsymbol{E}_B^{SC} = \hat{\boldsymbol{x}} E^{inc} k^2 \times \frac{\frac{a_{Wire}}{\varepsilon_0} - 2\boldsymbol{sign}(\boldsymbol{d})\eta a_{Wire} a_{SRR} v e^{-jkd} - a_{SRR} e^{-j2kd}}{1 + \mu_0 a_{Wire} a_{SRR} v^2} G(|z|),$$

$$\boldsymbol{E}_F^{SC} = \hat{\boldsymbol{x}} E^{inc} k^2 \times \frac{\frac{a_{Wire}}{\varepsilon_0} + a_{SRR} + 2i\eta\boldsymbol{sign}(\boldsymbol{d}) v a_{Wire} a_{SRR} Sin(kd)}{1 + \mu_0 a_{Wire} a_{SRR} v^2} G(|z|). \quad (6)$$

The first expression in Eq. (6) explicitly shows the degree of asymmetry in the back scattered field ($\boldsymbol{E}_B^{SC}$). This fact is manifested by the dependence on the sign of d that determines the HMEP orientation; for positive (negative) d, the incident plane wave hits the wire (SRR) first. At the same time, the forward scattering remains the same for both incident plane wave directions of propagation. This result could be also obtained by applying Lorentz reciprocity theorem. It may be insightful to examine the dependencies of the backward and forward scattered far-field on the various physical parameters of the system. First, note that the denominators of both $\boldsymbol{E}_F^{SC}$ and $\boldsymbol{E}_B^{SC}$ possess precisely the same form, and this form is even with d. In contrast, the numerator of $\boldsymbol{E}_B^{SC}$ depends nonlinearly on the individual polarizabilities while that of $\boldsymbol{E}_F^{SC}$ is linear with the polarizabilities. Furthermore, the phase of the various terms in the numerator of $\boldsymbol{E}_B^{SC}$ depends strongly on d and on its sign; hence, their mutual interference may differ considerably with the change of the sign of d and as well as with the change of the magnitude of d.

While the theoretical treatment above is exact for subwavelength structures of the ED and the MD, additional multipole terms need to be taken into account when their structure's size becomes comparable with the wavelength. Furthermore, the finite dimensions of the particles start to play a role in the case of small separation distances (d). Instead of using the multipolar expansion, which may become involved for numerous terms, the scattered field could be calculated numerically. This approach is undertaken ahead using CST Microwave Studio. In order to apply Eq. (6) and calculate the asymmetry factor, wire and SRR polarizabilities (a_{Wire}, a_{SRR}) should be obtained first. For this purpose, full wave simulations on individual elements (wire and SRR) were performed, and numerical values of polarizabilities were extracted from backscattered fields (e.g., a_{Wire} was obtained from Eq. (6) by putting $a_{SRR} = 0$, $d = 0$). Fig. 2 summarizes the results for the structure in a free space (dipole—thin strip 22.3×2 mm, SRR—outer diameter—8.3 mm, inner 6.3 mm, the gap—0.5 mm). Since substrates could introduce secondary contributions, such as resonance shifts, image secondary sources, and losses, they were omitted from those theoretical investigations, aiming on underlining the main effect. The asymmetry factor was defined as a ratio between the difference and the sum of backward scatterings at the opposite direction of incidence ($\pm\boldsymbol{k}$) (or changing the sing of d, while keeping the incident wave constant) $(|\boldsymbol{E}_B^{SC}(\boldsymbol{d}>0, z\to\infty)|^2 - |\boldsymbol{E}_B^{SC}(\boldsymbol{d}<0, z\to\infty)|^2)/(|\boldsymbol{E}_B^{SC}(\boldsymbol{d}>0, z\to\infty)|^2 + |\boldsymbol{E}_B^{SC}(\boldsymbol{d}<0, z\to\infty)|^2)$. This asymmetry factor is bounded between ± 1 similar to visibility coefficients, characterizing interference fringes.

The asymmetry factor (Fig. 2(a)) shows a strong dependence on the system's parameters—illumination frequency and the separation distance between the ring and the wire. First, the strong asymmetry could be achieved with subwavelength dimensions (Fig. 2(b))—here the near-field coupling has a crucial importance (e.g., for maximal asymmetry, the numerator of the first Eq. (6) vanishes). This property is unobtainable without employing a combination of electric and magnetic resonances, which is the unique property of the HEMP particle. The asymmetry also preserves at wavelength-comparable separation distances, Fig. 2(c)). An additional and a very remarkable feature is the strong sensitivity of the asymmetry factor on the separation distance—as it can be seen from Fig. 2(a)), a small change in d (on the scale of millimeters—less than one tenth of the wavelength) could flip the sign of the asymmetry coefficient. Likewise, the magnitudes and phases of the ED and the MD are very sensitive to both separation distance and frequency too. Furthermore, their specific values determine the far-field interference between the ED and MD fields, and hence also the asymmetry (supplementary material, Figs. S1 and S2 for further

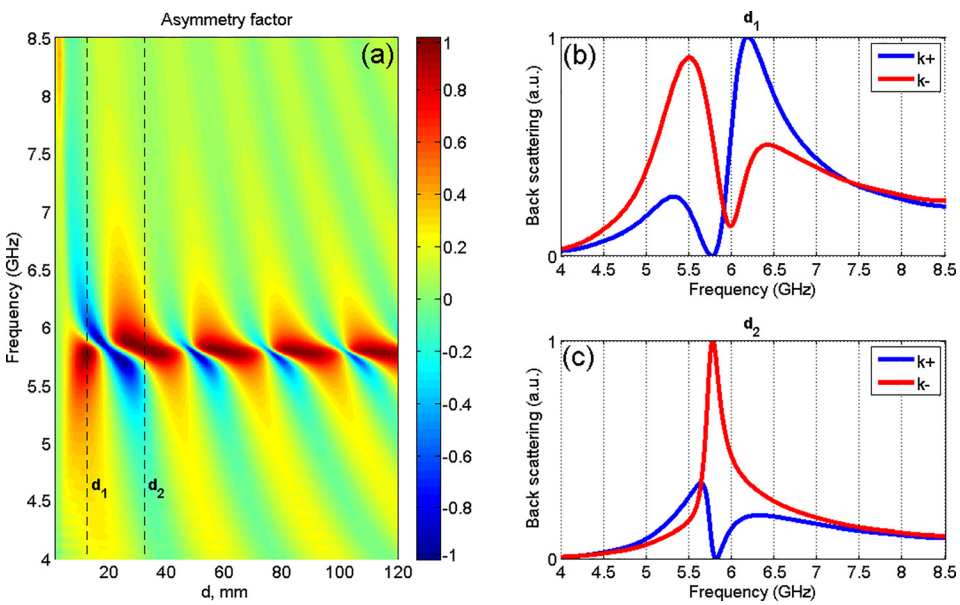

FIG. 2. Asymmetry in backward scattering from HEMP particles. (a) Asymmetry factor (color map) as the function of frequency of the incident wave and the separation distance between the dipole and the SRR (both assumed to be point particles in comparison to the separation distance), forming the HEMP. (b), (c) Back scattering spectra of HEMPs with fixed dimensions ($\boldsymbol{d}_1 = 10.5$ mm, $\boldsymbol{d}_2 = 32.3$ mm). Blue and red curves correspond to the opposite direction of incidence, indicated in Fig. 1. Sizes of the HEMP elements—(dipole—thin strip of 22.3×2 mm, SSR—outer diameter -8.3 mm, inner 6.3 mm, the gap -0.5 mm).

details). Such a high sensitivity could be employed, e.g., for sensing applications.

The photographic image of the fabricated HMEP particle appears in Fig. 1(b). The design of the constitutive elements is based on the standard copper strips, printed on a dielectric substrate (FR4 fiberglass, having $\varepsilon \approx 4.4$). In order to investigate asymmetric backscattering from HMEP, its basic components (the SRR and the wire) are analyzed first. Numerical simulations were performed with the frequency domain finite element method, implemented in CST Microwave Studio, aiming to emulate the experimental layout as close as possible, including the substrate effects. In order to implement the plane wave excitation in the laboratory conditions and measure the signal scattered to both the forward and backward directions, a pair of rectangular linearly polarized wideband horn antennas (1–18 GHz) were employed. Antennas were connected to the coaxial ports of a vector network analyzer (Agilent E8362B), able to extract both the amplitude and phase of the received signals. The experiment was conducted in an anechoic chamber where the HMEP was positioned in the far-field of the antennas. The distance from the HMEP to the transmitting and receiving antennas was approximately 1.5 m. The backscattering was extracted from the measured complex-valued signals, obtained in several steps in order to eliminate instrumental responses. The calibration was performed with a large area metallic mirror, having a reflection coefficient equal to -1. All the reflected signals were normalized accordingly to factorize the impact of the measurement apparatus. Both numerical and experimental data on constitutive HMEP elements appear at the supplementary material, Section 2.

Figs. 3(a) and 3(b) show the numerical values of forward and total scattering cross sections of the entire structure, depicted in Fig. 1. Blue and red lines correspond to the opposite directions of the incident plane wave. It can be seen that for both positive and negative $\boldsymbol{k}$ (or d), the scattering measures remain the same. Those numerical results underline the validity of the optical theorem, relating forward scattering to the RCS. As it could be explicitly seen, the theorem is satisfied, and no distinction on the propagation direction could be made. Figs. 3(c) and 3(d) show the main result, showing that the backscattering on the z axis at a large distance away from the HMEP, strongly depends on the direction of incident field propagation. In the forward direction (+k), the field is strongly reflected around 4 GHz, whereas in the backward direction (-k) there is almost no backscattering at the same frequency range. In order to satisfy the optical theorem, the scattered radiation should be redistributed along other directions in space. This behavior is explicitly shown in the inset of Fig. 4(c), where the polar plots of scattering diagrams appear. As it may be seen in the +k case, the backward scattering is quite significant, and it vanishes once the incidence direction is flipped. Scattering to sides of the HEMP increases on the expense of the backscattering. Fig. 3(d) shows the experimental data on the asymmetric scattering, and it is in an excellent agreement with the numerical investigations. Furthermore, the numerical results (geometry that includes the substrate) and theoretical predictions (Fig. 2) are in a very good agreement either—spectral behavior of curves is alike apart from a resonance shift, caused by the substrate. This effect suggests this meta-particle to be a valuable building block for different metamaterials that could benefit from asymmetric response to different incident field propagation directions.

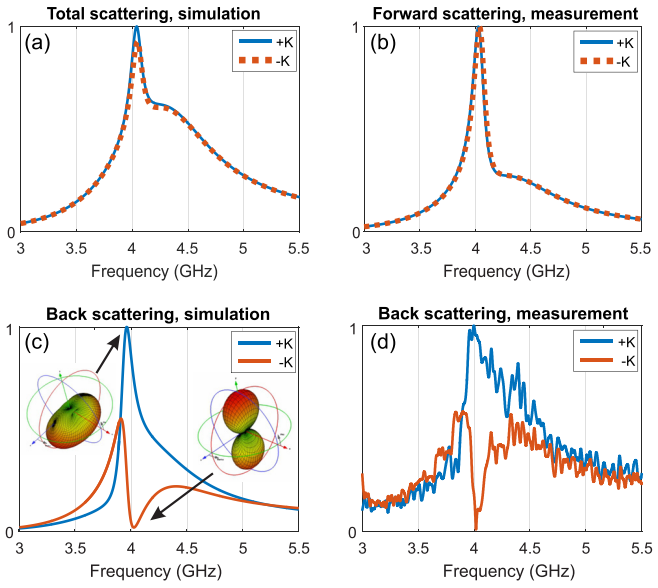

FIG. 3. HMEP particle, different directions of the incident plane wave. Numerical values of the total scattering cross section (a) and the forward scattering (b) spectra. Propagation direction on panels (a) and (b) is indistinguishable. (c) Numerical spectra of backscattered field. Insets—scattering patterns (polar plots) for different directions of incidence at 4 GHz. (d) Experimental spectra of the backscattered fields.

Fig. 4 shows the numerical simulations of the scattered fields from the HMEP. It may be seen that at the maximal asymmetry case (at 4 GHz), the backscattered field is almost vanished for one direction (Fig. 4(a)), whereas in the opposite case it even predominates the forward scattering (Fig. 4(b)). Boundaries of wire, ring, and the substrate could be clearly seen on the fields map. It is worth noting that the asymmetry is preserved with changing the particle's rotation angle. The maximal ratio, however, is obtained for the case, when the k-vector of the incident wave is co-planar with the particle major axis (line, connecting the wire and the ring) (supplementary material, Section 3 for further information).

For summary, the HMEP meta-particle was analyzed analytically, numerically, and experimentally, and was shown to have strong asymmetric response—being illuminated from opposite directions, it has completely symmetric forward scattering, while maximum asymmetry was achieved in the

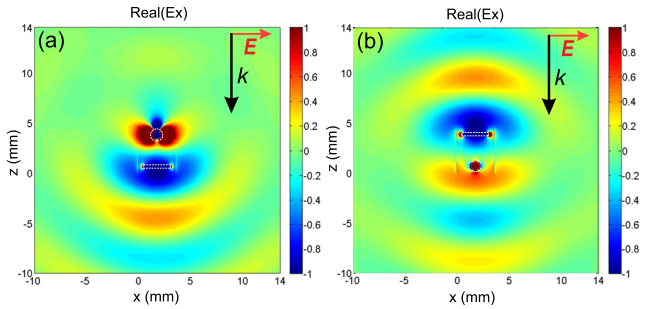

FIG. 4. Color maps of the scattered fields (real part of phasors) for opposite propagation directions (a) and (b). HMEP dimensions are the same as in Fig. 3, operation frequency is 4 GHz. White dashed lines represent physical boundaries on the wire and the ring.

backward direction. The backscattering from the particle may be as low as 0 for one direction of the incident wave, while being maximal at the same frequency range for the opposite direction of propagation. It should be underlined that the optical theorem is not violated, and the scattered signal is merely redistributed between the other directions in space.

One of the fundamental properties of Maxwell's equations is that they are frequency scalable—this means that scattering from meta-atoms designed for the optical frequencies would be analogous to scattering from a similar meta-atom designed for radio frequencies (RF), provided that the material parameters μ and ε are the same.[31] This scalability enables the emulation of optical metamaterials, which are often difficult to fabricate due to their small dimensions, with the relatively easily manufacturable metamaterials in the RF range.[32,33] Therefore, the proposed structure could be employed for approaching a range of applications in the optical domain. Consequently, HMEP could be used as a building block for asymmetric metamaterials assembling parts of solar cells, optical diodes, and many others.

See supplementary material for three sections—"Phase relation of the electric and magnetic dipoles," "Numerical and experimental retrieval of polarizabilities of standalone particles," and "Angular dependence of scattering characteristics,"

This work was supported, in part, by TAU Rector Grant and German-Israeli Foundation (GIF, Grant No. 2399) and by the Russian Fund for Basic Research within the Project No. 16-52-00112. The analytical calculation of multipolar terms of meta-particle has been supported by the Russian Science Foundation Grant No. 16-12-10287. A.S.S. acknowledges the support of the President of Russian Federation in the frame of Scholarship SP-4248.2016.1 and the support of Ministry of Education and Science of the Russian Federation (GOSZADANIE 2014/190). The authors acknowledge Dr. Tal Ellenbogen (Tel Aviv University) for discussions.

[1]R. W. Z. Nader Engheta, *Metamaterials: Physics and Engineering Explorations* (Wiley-IEEE Press, 2006).
[2]Y. Wang, T. Sun, T. Paudel, Y. Zhang, Z. Ren, and K. Kempa, "Metamaterial-plasmonic absorber structure for high efficiency amorphous silicon solar cells," Nano Lett. **12**(1), 440–445 (2012).
[3]D. Schurig, J. J. Mock, B. J. Justice, S. A. Cummer, J. B. Pendry, A. F. Starr, and D. R. Smith, "Metamaterial electromagnetic cloak at microwave frequencies," Science **314**(5801), 977–980 (2006).
[4]S. Larouche, Y. Tsai, T. Tyler, N. M. Jokerst, and D. R. Smith, "Infrared metamaterial phase holograms," Nat. Mater. **11**(5), 450–454 (2012).
[5]A. S. Shalin, S. V. Sukhov, A. A. Bogdanov, P. A. Belov, and P. Ginzburg, "Optical pulling forces in hyperbolic metamaterials," Phys. Rev. A **91**, 063830 (2015).
[6]A. A. Bogdanov, A. S. Shalin, and P. Ginzburg, "Optical forces in nanorod metamaterial," Sci. Rep. **5**, 15846 (2015).
[7]B. Sauviac, C. R. Simovski, and S. A. Tretyakov, "Double split-ring resonators : Analytical modeling and numerical simulations," Electromagnetics **24**(5), 317–338 (2004).
[8]O. Sydoruk, "Tailoring the near-field guiding properties of magnetic metamaterials with two resonant elements per unit cell," Phys. Rev. B **73**, 224406 (2006).
[9]Y. Hadad and B. Z. Steinberg, "Electrodynamic synergy of micro-properties and macro-structure in particle arrays," in *URSI International Symposium on Electromagnetic Theory* (2010), pp. 680–683.
[10]A. O. Karilainen and S. A. Tretyakov, "Isotropic chiral objects with zero backscattering," IEEE Trans. Antennas Propag. **60**(9), 4449–4452 (2012).
[11]D. S. Filonov, A. P. Slobozhanyuk, P. A. Belov, and Y. S. Kivshar, "Double-shell metamaterial coatings for plasmonic cloaking," Phys. Status Solidi RRL **6**(1), 46–48 (2012).
[12]K. X. Wang, Z. Yu, S. Sandhu, V. Liu, and S. Fan, "Condition for perfect antireflection by optical resonance at material interface," Optica **1**(6), 388 (2014).
[13]K. Tvingstedt, S. D. Zilio, O. Inganäs, and M. Tormen, "Trapping light with micro lenses in thin film organic photovoltaic cells," Opt. Express **16**(26), 21608–21615 (2008).
[14]T. Shegai, S. Chen, V. D. Miljković, G. Zengin, P. Johansson, and M. Käll, "A bimetallic nanoantenna for directional colour routing," Nat. Commun. **2**, 481 (2011).
[15]Y. Liu and X. Zhang, "A new frontier of science and technology," Chem. Soc. Rev. **40**, 2494–2507 (2011).
[16]A. P. Slobozhanyuk, P. V. Kapitanova, D. S. Filonov, D. A. Powell, I. V. Shadrivov, M. Lapine, P. A. Belov, R. C. McPhedran, and Y. S. Kivshar, "Nonlinear interaction of meta-atoms through optical coupling," Appl. Phys. Lett. **104**(1), 014104 (2014).
[17]I. V. Shadrinov, V. A. Fedotov, D. A. Powell, Y. S. Kivshar, and N. I. Zheludev, "Electromagnetic wave analogue of an electronic diode," New J. Phys. **13**, 033025 (2011).
[18]A. E. Krasnok, A. E. Miroshnichenko, P. A. Belov, and Y. S. Kivshar, "All-dielectric nanoantennas," Proc. SPIE **8806**, 880626 (2013).
[19]A. O. Karilainen, P. Alitalo, and S. A. Tretyakov, "Chiral antenna element as a low backscattering sensor," in *EUCAP 5th European Conference on Antennas and Propagation (EuCAP 2011)*, Rome, Italy, April 11–15, 2011, pp. 1983–1986.
[20]W. Liu, A. E. Miroshnichenko, D. N. Neshev, and Y. S. Kivshar, "broadband unidirectional scattering by magneto-electric core–shell nanoparticles," ACS Nano **6**(6), 5489–5497 (2012).
[21]Y. Ra'di, S. Member, V. S. Asadchy, and S. A. Tretyakov, "Total absorption of electromagnetic waves in ultimately thin layers," IEEE Trans. Antennas Propag. **61**(9), 4606–4614 (2013).
[22]Y. Ra'di, S. Member, V. S. Asadchy, and S. A. Tretyakov, "Tailoring reflections from thin composite metamirrors," IEEE Trans. Antennas Propag. **62**(7), 3749–3760 (2014).
[23]Y. Ra, V. S. Asadchy, and S. A. Tretyakov, "One-way transparent sheets," Phys. Rev. B **89**, 075109 (2014).
[24]V. V. Klimov, I. V. Treshin, A. S. Shalin, P. N. Melentiev, A. A. Kuzin, A. E. Afanasiev, and V. I. Balykin, "Optical Tamm state and giant asymmetry of light transmission through an array of nanoholes," Phys. Rev. A **92**(6), 63842 (2015).
[25]C. Pfeiffer and A. Grbic, "Metamaterial Huygens' surfaces: Tailoring wave fronts with reflectionless sheets," Phys. Rev. Lett. **110**(19), 197401 (2013).
[26]J. D. Jackson, *Classical Electrodynamics*, 3rd ed. (Wiley, New York, 1999), pp. 174ff, 775ff.
[27]S. Gupta, L. J. Jiang, S. Member, and C. Caloz, "Magneto-electric dipole antenna arrays," IEEE Trans. Antennas Propag. **62**(7), 3613–3622 (2014).
[28]C. R. Simovski, P. A. Belov, and S. He, "Backward wave region and negative material parameters of a structure formed by lattices of wires and split-ring resonators," IEEE Trans. Antennas Propag. **51**(10), 2582–2591 (2003).
[29]L. Novotny and H. Bert, *Principles of Nano-Optics* (Cambridge University Press, 2006).
[30]D. Markovich, K. Baryshnikova, A. Shalin, A. Samusev, A. Krasnok, P. Belov, and P. Ginzburg, "Enhancement of artificial magnetism via resonant bianisotropy," Sci. Rep. **6**, 22546 (2016).
[31]B. Hopkins, D. S. Filonov, S. B. Glybovski, and A. E. Miroshnichenko, "Hybridization and the origin of Fano resonances in symmetric nanoparticle trimers," Phys. Rev. B: Condens. Matter Mater. Phys. **92**(4), 045433 (2015).
[32]D. S. Filonov, A. S. Shalin, I. Iorsh, P. A. Belov, and P. Ginzburg, "Controlling electromagnetic scattering with wire metamaterial resonators," J. Opt. Soc. Am. A **33**(10), 1910 (2016).
[33]P. V. Kapitanova, P. Ginzburg, F. J. Rodríguez-Fortuño, D. S. Filonov, P. M. Voroshilov, P. A. Belov, A. N. Poddubny, Y. S. Kivshar, G. A. Wurtz, and A. V Zayats, "Photonic spin Hall effect in hyperbolic metamaterials for polarization-controlled routing of subwavelength modes," Nat. Commun. **5**, 3226 (2014).